MARTIN MARIETTA ENERGY SYSTEMS LIBRARIES

3 4456 0381866 1

ORNL/TM-12730

ornl

OAK RIDGE NATIONAL LABORATORY

MARTIN MARIETTA

Design and Construction of the Astronautics Refrigerator Magnet

Lawrence Dresner

OAK RIDGE NATIONAL LABORATORY
CENTRAL RESEARCH LIBRARY
CIRCULATION SECTION
4500N ROOM 175
LIBRARY LOAN COPY
DO NOT TRANSFER TO ANOTHER PERSON
If you wish someone else to see this report, send in name with report and the library will arrange a loan.

MANAGED BY
MARTIN MARIETTA ENERGY SYSTEMS, INC.
FOR THE UNITED STATES
DEPARTMENT OF ENERGY

This report has been reproduced directly from the best available copy.

Available to DOE and DOE contractors from the Office of Scientific and Technical Information, P.O. Box 62, Oak Ridge, TN 37831; prices available from (615) 576-8401, FTS 626-8401.

Available to the public from the National Technical Information Service, U.S. Department of Commerce, 5285 Port Royal Rd., Springfield, VA 22161.

This report was prepared as an account of work sponsored by an agency of the United States Government. Neither the United States Government nor any agency thereof, nor any of their employees, makes any warranty, express or implied, or assumes any legal liability or responsibility for the accuracy, completeness, or usefulness of any information, apparatus, product, or process disclosed, or represents that its use would not infringe privately owned rights. Reference herein to any specific commercial product, process, or service by trade name, trademark, manufacturer, or otherwise, does not necessarily constitute or imply its endorsement, recommendation, or favoring by the United States Government or any agency thereof. The views and opinions of authors expressed herein do not necessarily state or reflect those of the United States Government or any agency thereof.

ORNL/TM-12730

Fusion Energy Division

DESIGN AND CONSTRUCTION OF THE ASTRONAUTICS REFRIGERATOR MAGNET

Lawrence Dresner

Date published: May 1994

Prepared for the
Office of Energy Efficiency and Renewable Energy
Budget Activity No. AK 06 00 00 0

Research conducted under
Cooperative Agreement No. 86X-SJ161V

Prepared by
OAK RIDGE NATIONAL LABORATORY
Oak Ridge, Tennessee 37831
managed by
MARTIN MARIETTA ENERGY SYSTEMS, INC.
for the
U.S. DEPARTMENT OF ENERGY
under contract DE-AC05-84OR21400

MARTIN MARIETTA ENERGY SYSTEMS LIBRARIES

3 4456 0381866 1

CONTENTS

LIST OF FIGURES v
LIST OF TABLES vii
ACKNOWLEDGMENTS ix
ABSTRACT 1
1. INTRODUCTION: SIZE AND SHAPE OF THE MAGNET 1
2. DETAILED DESIGN OF THE WINDING 2
3. PROTECTION 3
4. OUT-OF-BORE FIELD REDUCTION BY SOFT IRON FLANGES 5
5. MAGNETIC FORCE BETWEEN THE BEDS AND THE MAGNET 7
6. HYSTERESIS LOSSES 8
7. COUPLING LOSSES 9
8. RADIAL DESTABILIZING FORCE ON THE BED IN THE MAGNET 10
9. LOCATION OF THE 5-GAUSS SURFACE 12
10. CONSTRUCTION OF THE MAGNET 12
REFERENCES 14

LIST OF FIGURES

Figure		Page
1	A sketch of the magnet and bed defining the conventional shape factors α and β	15
2	The values of α and β that minimize $(\alpha^2 - 1)\beta$ plotted against $F(\alpha, \beta) = B_o/\mu_o Ja$	16
3	The minimum value of $(\alpha^2 - 1)\beta$ plotted against $F(\alpha, \beta) = B_o/\mu_o Ja$	17
4	The quantity $c\sqrt{i}$ plotted versus i [c is defined in Eq. (4b)]	18
5	A sketch of the magnet showing one of the soft iron end-flanges used as flux returns	19
6	The calculated on-axis field as a function of distance from the magnet center with and without the soft iron end-flanges	20
7	The saturation magnetization of $GdNi_2$ as a function of temperature with field as a parameter	21
8	The total force on a pair of rigidly connected beds as a function of the displacement of one of them from the center	22
9	An auxiliary sketch to aid in the interpretation of the curves in Fig. 8	23
10	A sketch showing the location of the current sheet that replaces the bed	24
11	A schematic depiction of the bed in the bore tube	25
12	A sketch of the bed assembly, support tubes, magnet, and bearings	25
13	The construction drawing of the magnet	26
14	A photograph of the completed magnet	27
15	A photograph of the closed helium pot showing the six tubes that connect the interior of the helium pot to the laboratory	28
16	The measured on-axis field as a function of distance from the magnet center with the soft iron end-flanges present	29

LIST OF TABLES

Table		Page
1	Specifications of the SSC wire	2
2	Critical current density data of Valaris and Kallsen	3
3	Specifications of a magnet wound with close-packed Formvar-insulated SSC strands	3
4	Specific heat parameters of NbTi and Cu	4
5	Results of field computation	11

ACKNOWLEDGMENTS

I would like to acknowledge the valuable assistance I received in many conversations with Dr. Anthony DeGregoria and Mr. Rick Lubasz, both earlier with ACA. I would also like to acknowledge the many useful improvements to my original design suggested by Messrs. Lanny Lewis, Ronald Efferson, and Stephen Elgin of American Magnetics, Inc. I would like to thank Dr. Richard Murphy of ORNL for bringing to my attention the radial destabilizing force on the bed in the magnet. Finally, I would like to acknowledge the help I received from my colleagues Dr. S. W. Schwenterly, Dr. J. W. Lue, and Mr. M. S. Lubell of the Magnetics and Superconductivity Section of FED/ORNL. The contributions of these people helped immeasurably to improve the design of the magnet, and I am grateful to each of them.

ABSTRACT

This document reports on the design, construction, and testing of a 7-Tesla, 4-in. bore superconducting magnet for use in the Astronautics Refrigerator Experiment. The magnet is a single-strand, layer-wound, potted solenoid wound with Formvar-insulated SSC strands. The magnet was constructed by American Magnetics, Inc. of Oak Ridge and has been installed in the Astronautics Refrigerator Experiment at the Astronautics Technology Center in Madison, Wisconsin.

1. INTRODUCTION: SIZE AND SHAPE OF THE MAGNET

The task was to design a solenoid that has a bore diameter $2a = 4$ in. = 10.16 cm and that produces a central field $B_0 = 7$ T. The first step is to determine the shape factors α and β (see Fig. 1 for the definitions of α and β). We do this by minimizing the winding volume as follows:

The field B at a point P on the axis of a solenoid is given by

$$B = \mu_0 J a \cdot \frac{1}{2}\left[F(\alpha, t_1) + F(\alpha, t_2)\right] \tag{1a}$$

where

$$t_1 = \beta - z/a \ , \quad t_2 = \beta + z/a \ , \tag{1b}$$

and

$$F(\alpha, t) = t \ln\left(\frac{\alpha + \sqrt{\alpha^2 + t^2}}{1 + \sqrt{1 + t^2}}\right) . \tag{1c}$$

Here z is the distance of P from the center of the magnet, μ_0 is the permittivity of free space ($4\pi \times 10^{-7}$ Henry/m), and J is the average current density over the winding. When $z = 0$, the central, on-axis field B_0 is given by

$$\frac{B_0}{\mu_0 J a} = F(\alpha, \beta) \ . \tag{2}$$

If we fix the value of J, the current density, we fix the value of the shape function $F(\alpha, \beta)$. For each value of F, there is a unique pair of shape factors (α, β) that minimizes the winding volume $V = 2\pi\,(\alpha^2 - 1)\beta a^3$. These α and β are shown in Fig. 2 plotted against F.

Shown in Fig. 3 is a plot of the minimum value of $(\alpha^2 - 1)\beta$ versus F. According to Fig. 3, $(\alpha^2 - 1)\beta$ varies as the 1.7-power of F, which means the winding volume V varies inversely as the 1.7-power of the current density J since B_0 and a are fixed by the design constraints.

To achieve low cost (and a small magnet), the current density should be high. But as current density increases, stability decreases. A current density of 15 kA/cm^2 is not an extravagant goal from the point of view of stability. With SSC strands (which we recently purchased at \$0.91 per meter), the cost of superconductor for the magnet would be about \$3,200. A crude rule of thumb is to triple the cost of the superconductor to get the cost of the magnet, which would then be about \$10,000. Reducing the current density to 5 kA/cm^2 would diminish the stability problem but would increase the cost by a factor of 6.5, making the magnet rather expensive. On the other hand, increasing the current density to 30 kA/cm^2, which is rather risky, would decrease the cost by less than a factor of three. I say "less than" because when the magnet is small, the rule of three quoted above probably no longer holds: a certain irreducible amount of labor is required to make the magnet, even if the superconductor inventory is very small. In view of the relatively small expected cost of the 15-kA/cm^2 magnet to start with, the risk of increasing the current density seems unjustified.

When $J = 15$ kA/cm^2, $F = B_0/\mu_0 Ja = 0.7310$, and the minimum-volume shape factors are $\alpha = 2.162$ and $\beta = 1.258$. The magnet dimensions are then these: OD = 8.647 in. = 21.96 cm, length = 5.027 in. = 12.77 cm, build = 2.323 in. = 5.902 cm. The volume of the winding is 3.803 L.

2. DETAILED DESIGN OF THE WINDING

To proceed further with the design, one must choose a conductor and decide how it will be wound and cooled. A convenient conductor, of which ORNL had an adequate supply on hand, is one produced for the Superconducting Super Collider (SSC). Its specifications are given in Table 1. The data used to determine the critical current density in Table 1 are reported by Valaris et al. in Ref. 1 and by Kallsen et al. in Ref. 2; they are listed in Table 2.

Table 1. Specifications of the SSC wire

Strand diameter	0.81 mm
Cu/NbTi volume ratio	1.5
Critical current density (7 T, 4.2 K)	1.8 kA/mm^2 of NbTi

The data in columns 2 and 3 of Table 2 are well fitted by a second-order polynomial in B (column 4), namely

$$J_c = \bar{a} + \bar{b}B + \bar{c}B^2 \tag{3}$$

where

$\bar{a} = 6.821$ kA/mm^2,
$\bar{b} = -0.8394$ kA/mm^2-T, and
$\bar{c} = 0.01726$ kA/mm^2-T^2.

Table 2. Critical current density data of Valaris and Kallsen

	J_c (4.2 K) (kA/mm^2 of NbTi)		
Magnetic field (T)	Valaris et al.	Kallsen et al.	Least squares
2		5.214	5.211
5	3.028	3.039	3.055
5.6	2.664		2.661
6	2.422	2.405	2.405
7	1.817	1.802	1.790
8		1.197	1.210

A single-strand, layer-wound, potted winding is a good choice for a small magnet such as that foreseen here. The specifications of the magnet are given in Table 3.

Table 3. Specifications of a magnet wound with close-packed Formvar-insulated SSC strands

Bore radius, cm	5.08
Outer diameter, cm	22.0
Length, cm	12.8
Area of winding, cm^2	75.4
Overall current density, kA/cm^2	15
Ampere-turns	1.13×10^6
Packing fraction	$\pi/2\sqrt{3} = 0.907$
Area of stands, cm^2	68.3
Number of turns	13,263
Critical current per strand (7 T, 4.2 K), A	371
Current per strand, A	85.2 (23% of critical)
Inductance, H	16.0
Stored energy, kJ	58.1
Total length of winding, km	6.69
Charge time at 6 V, s	77.7

3. PROTECTION

The magnet described above is self-protecting. This means that if a normal zone were formed at a point, say by cracking of the epoxy, it would grow quickly enough that the stored energy would be more or less uniformly spread over the mass of the magnet. The subsequent rise in temperature would then be well within tolerable limits.

In an uncooled conductor, the longitudinal velocity of propagation is given by

$$v = c(i)\sqrt{i}\ \frac{J_c}{S}\left(\frac{L_0 T_b}{T_c - T_b}\right)^{1/2} \tag{4a}$$

where the function $c(i)$ is determined by Eq. (4b) [3]:

$$\frac{c}{\sqrt{4 - c^2}}\ \arctan\left(\frac{c\sqrt{4 - c^2}}{2 - c^2}\right) + 2\ln c = \ln\left(\frac{i}{1 - i}\right) . \tag{4b}$$

The quantity $c\sqrt{i}$ is shown in Fig. 4 plotted versus i. Shown also is the straight line of slope 1 through the origin. For $i < 0.3$, the curve and the line are very close, so that $c\sqrt{i} \approx i$, in which case Eq. (4a) becomes

$$v = \frac{J}{S}\left(\frac{L_0 T_b}{T_c - T_b}\right)^{1/2} . \tag{4c}$$

For S we must write

$$S = f\,\delta_{\mathrm{Cu}} C_{p\mathrm{Cu}} + (1-f)\,\delta_{\mathrm{NbTi}} C_{p\mathrm{NbTi}} \tag{5a}$$

where the specific heat is given by

$$C_p = \hat{\gamma} T + \hat{\beta} T^3 \tag{5b}$$

where the values of $\hat{\beta}$, $\hat{\gamma}$, and δ are listed in Table 4.

Table 4. Specific heat parameters of NbTi and Cu

	NbTi [4]	Cu [5]	Units
$\hat{\gamma}$	0.145	0.011	J/kg-K^2
$\hat{\beta}$	2.3×10^{-3}	7.44×10^{-4}	J/kg-K^4
δ	6000	8960	kg/m^3

Since $f = 0.6$ according to the data in Table 1, for the SSC strands

$$S = \hat{c}\,T + \hat{b}\,T^3 \tag{6a}$$

where

$$\hat{c} = 407\ \mathrm{J/m^3\text{-}K^2}\ , \quad \hat{b} = 9.52\ \mathrm{J/m^3\text{-}K^2}\ . \tag{6b}$$

According to Eq. (6), the average specific heat in the range (T_b, T_c), where $T_b = 4.2$ K and $T_c = 6.0$ K (7 T) is $S = 3380$ J/m^3-K. The value of J in the strands 16.5 kA/cm^2. Then according to Eq. (4c), the propagation velocity is 11.7 m/s.

This is the longitudinal propagation velocity. The transverse propagation velocity is smaller by a factor $(S_{\|}/S_{\perp})(k_{\perp}/k_{\|})^{1/2}$, where $k_{\perp}$ and $k_{\|}$ are the thermal conductivities of the winding in the transverse and longitudinal directions, respectively, and $S_{\perp}$ and $S_{\|}$ are the volumetric heat capacities per unit volume with and without the contribution of the epoxy, respectively. Since copper is the continuous phase in the strands and is expected to have a much larger thermal conductivity than normal-state NbTi, a binary alloy, we calculate $k_{\perp}$ as though the copper and epoxy were thermally in series and the NbTi were replaced by vacuum. Thus

$$k_{\perp} = \left[\frac{f_{ep}}{k_{ep}} + \frac{\left(1 - f_{ep}\right)^2}{k_{\mathrm{Cu}} f_{\mathrm{Cu}}}\right]^{-1} \; ; \quad k_{\|} = \frac{k_{\mathrm{Cu}} f_{\mathrm{Cu}}}{f_{\mathrm{Cu}} + f_{\mathrm{NbTi}}} \tag{7}$$

where the f's are volume fractions ($f_{ep} = 0.0931, f_{\mathrm{Cu}} = 0.5441, f_{\mathrm{NbTi}} = 0.3628$) and the k's are thermal conductivities. According to Reed and Clark [5], $k_{ep} \approx 0.1$ W/m-K and $(C_p) \approx 1$ J/kg-K. We take $\delta_{ep} = 1000$ kg/m^3. We find k_{Cu} from the Wiedemann-Franz law assuming for the copper $\rho = 5.39 \times 10^{-10}$ ohm-m [RRR = 79 (Ref. 6); the resistivity includes magnetoresistivity]. We then find $k_{\mathrm{Cu}} = 191$ W/m-K. From Eq. (7) it follows that $k_{\perp} = 1.065$ W/m-K and $k_{\|} = 115$ W/m-K so that $(k_{\perp}/k_{\|})^{1/2} = 0.0964$. Furthermore, $S_{\perp}/S_{\|} = 1 + 1000 \times 0.0931/3380 \times 0.9069 = 1.030$. Therefore, the ratio of the transverse to the longitudinal propagation velocities is 0.0936. The transverse velocity is then of the order of 1 m/s, and the entire coil will become normal in about 0.1 s.

The adiabatic hot-spot integral $\int_0^{0.1\,\mathrm{s}} J^2 dt = 2.25 \times 10^{15}\,\mathrm{A}^2\mathrm{m}^{-4}\mathrm{s}$ and corresponds to a hot-spot temperature of about 20 K. If the stored energy (58.1 kJ) of the coil were uniformly spread over the entire conductor volume (3.08 L), the final temperature would be 53 K, according to the enthalpy derived from Eq. (6). The hot-spot temperature is then less than 73 K, which is entirely tolerable.

4. OUT-OF-BORE FIELD REDUCTION BY SOFT IRON FLANGES

Soft iron flanges placed on the ends of the magnet serve as flux return paths and so may be expected to decrease the field experienced by the bed when it is fully withdrawn from the magnet. We can roughly estimate the size and effect of such flanges as follows.

To begin with, let us assume the iron to be completely saturated in the high fields present at the ends of the magnet and let us take the saturation magnetization M in the iron to be 2 T [$B = \mu_0(H + M)$; $\mu_0 M = 2$ T]. We estimate the thickness of the flanges by assuming the entire flux from the bore returns through the iron (Fig. 5). Then

$$\pi a^2 B_0 = 2\pi a(\gamma - \beta) a \mu_0 M \tag{8a}$$

or

$$\gamma = \beta + B_0/2\mu_0 M \tag{8b}$$

which corresponds to a flange 8.89 cm (3.50 in.) thick.

Now an infinite slab of saturated iron with a magnetization M can be replaced by two oppositely directed current sheets whose current per unit length I is equal to the magnetization M, i.e., $I = M$. We propose to replace the flanges by such current sheets in order to estimate their effect. Since the magnetization M of the flanges is radially outwards, the sheet currents must flow azimuthally as shown in Fig. 5. Such annular current sheets are just thin solenoids in planes AB and CD. This replacement is only approximate, but should suffice for us to estimate the effect of the flanges.

The on-axis field of a solenoid is given by Eq. (1). We need to specialize these formulas to the limit $\beta \to 0$ while βJa remains fixed at the value $I/2$. Since F is an odd function of t, we can write Eq. (1a) as

$$B = \mu_0 Ja \cdot \frac{1}{2}\left[F(\alpha,\ z/a + \beta) - F(\alpha,\ z/a - \beta)\right] \tag{9a}$$

which becomes in the limit,

$$B = \frac{\mu_0 I}{2}\left(\frac{\partial F}{\partial t}\right)_{t=z/a} = \frac{\mu_0 M}{2}\left(\frac{\partial F}{\partial t}\right)_{t=z/a} . \tag{9b}$$

From Eq. (1c) we find that

$$\frac{\partial F}{\partial t} = G(\alpha,\ t) - G(1,\ t) \tag{10a}$$

where

$$G(\alpha,\ t) = \ln\left(\alpha + \sqrt{\alpha^2 + t^2}\right) + \frac{t^2}{\left(\alpha + \sqrt{\alpha^2 + t^2}\right)\sqrt{\alpha^2 + t^2}} . \tag{10b}$$

The field contribution from the sheet AB adds to that of the main magnet; the contribution from the sheet CD subtracts.

The magnet described in Table 3 has $J = 1.5 \times 10^8$ A/m^2, $a = 0.0508$ m, $\alpha = 2.162$, and $\beta = 1.258$. According to Eq. (8b), $\gamma = 3.008$. Figure 6 shows its on-axis field with and without end flanges. The out-of-bore field at the bed is substantially educed by the presence of the iron flange.

5. MAGNETIC FORCE BETWEEN THE BEDS AND THE MAGNET

The force per unit volume $\vec{f}$ exerted on a magnetized bed (magnetization $\vec{M}$) by the field $\vec{B}$ of the magnet is given by

$$\vec{f} = \nabla\left(\vec{M}\cdot\vec{B}\right) \tag{11a}$$

where the ∇ operates only on $\vec{B}$. At low temperatures, the magnetization of the bed material, $GdNi_2$, saturates at quite low fields; for example, at 40 K, it saturates for applied fields of less than 1 T at roughly 125 A-m^2/kg (see Fig. 7). Since the density of $GdNi_2$ is 9680 kg/m^3, 1 A-m^2/kg thus corresponds to a magnetization of 9680 A/m, which contributes 12.2 mT to the magnetic induction B. Therefore, 125 A-m^2/kg corresponds to a saturation induction $\mu_o M$ of 1.52 T. Assuming $\vec{M}$ to be parallel to $\vec{B}$, Eq. (11a) becomes

$$\vec{f} = M\nabla B \tag{11b}$$

The total force $\vec{F}$ on the bed is then

$$\vec{F} = \iiint_{\substack{\text{bed}\\ \text{vol.}}} \vec{f}\, d(\text{vol}) = M\iiint_{\substack{\text{bed}\\ \text{vol.}}} \nabla B\, d(\text{vol}) = \iiint_{\substack{\text{bed}\\ \text{surf.}}} B\vec{n}\, d(\text{surf}) \quad . \tag{12a}$$

The lateral surfaces of the bed contribute nothing to the integral because of the azimuthal symmetry both of the bed and the field. Hence, the force is axial, attractive, and of magnitude

$$F = \frac{(\mu_o M)\Delta B}{\mu_o}\,\pi a^2 \tag{12b}$$

where ΔB is the difference in B between the two ends of the bed. Equation (12b) is based on the assumption that the field is uniform over the end faces of the bed and equal to the on-axis field.

In using Eq. (12b), it is necessary to account for the voids in the bed; the packing fraction is 56%, which reduces the effective value $\mu_o M$ to 0.851 T.

Figure 8 shows the total force on a pair of rigidly connected beds (each 5 cm in diameter and 5 cm long) as a function of the displacement of one of them from the magnet center. The parameter labeling the curves is the bed separation in cm. Except for the curve corresponding to the smallest separation, all the curves have a sinusoidal shape. Consider, for a moment, the curve corresponding to a separation of 20 cm. When the distance of bed 1 from the center is $z = 0$, the distance of bed 2 from the center is $z = 20$ cm. The force on bed 1 is zero (by symmetry); that on bed 2 is very small because it is far from the magnet center (point A in Fig. 9). At point B, the force tending to pull bed 1 back into the magnet is large while that on bed 2 is still small. At point C, the forces on the two beds are balanced and the net force is zero. Point D is like point B, but with the

direction of the force reversed, and point E is like point A, but with the direction of the force reversed. A similar analysis holds for the other curves.

If the bed separation is 17.5 cm and the bed stroke about 20 cm (to minimize the field on the bed not in the magnet), the maximum force on the bed assembly is about 4000 N (or 900 lb.).

6. HYSTERESIS LOSSES

The motion of the paramagnetic bed into and out of the bore of the magnet induces a voltage across the winding that is opposed by a change in the magnet current. The change in current alters the field of the magnet and thereby causes hysteresis losses in the superconducting filaments.

A paramagnetic bed in the fully inserted position has a saturated magnetization M of 6.77×10^5 A/m (which corresponds to an induction of 0.851 T). Since the bed is a cylinder whose axis is parallel to the magnetization vector, it is equivalent to a sheet current on its outer cylindrical surface whose linear density $I = M$ (see Fig. 10). We now replace the problem of inserting the bed with another problem, namely, that of charging the sheet current $I = M$ with the bed already in the inserted position. These problems are not the same, but should have roughly the same hysteresis losses. This replacement is unavoidable because the actual problem is extremely difficult and would involve quite long and extensive computations.

The magnet, being superconducting, cannot support any voltage, so that as the current sheet is being charged

$$L \frac{dI}{dt} + M_s \frac{d}{dt}(2zM) = 0 \tag{13}$$

where L is the self-inductance of the magnet, M_s is the mutual inductance between the one-turn current sheet and the magnet, and z is the half-length of the bed. Integrating Eq. (13) with respect to time over half a cycle, we find that the absolute change in the magnet current on fully charging the current sheet is

$$|\Delta I| = 2zM \frac{M_s}{L} \ . \tag{14}$$

The inductances have been determined by the Fawzi-Burke method [6]; $L = 16.0$ H and $M_s = 700$ μH. Then from Eq. (14), we find $|\Delta I| = 1.48$ A. Since the operating current of the magnet is 85.2 A, $|\Delta I/I| = 0.0174$.

The hysteresis power density in a fully saturated round filament of diameter D is $2J_c|dB/dt|\, D/3\pi$. Thus, the total dissipation Q per cycle per bed is

$$Q = \frac{4}{3\pi} J_c|\Delta B|DV = \frac{4}{3\pi} \frac{|\Delta I|}{I} (J_c B)VD \tag{15}$$

where V is the volume of the superconductor (NbTi) in the magnet (1.38 L). Now for the SSC conductor, J_cB is roughly constant at about 12 kA-T/mm^2 and $D = 6$ μm. Therefore, $Q = 0.734$ J per cycle per bed. Since there are two beds and the cycle time is 2 s, the average hysteresis power is 0.734 W.

7. COUPLING LOSSES

The coupling-loss power density $\dot{Q}$ in a composite strand is given by

$$\dot{Q} = \frac{\dot{B}^2}{\rho}\left(\frac{p}{2\pi}\right)^2 \tag{16}$$

where $\dot{B}$ is the rate of change of the magnetic field, ρ is the transverse (matrix) resistivity, and p is the twist pitch of the filaments. Now $\dot{B} = \Delta B/\Delta t$, where ΔB is the field change caused by insertion or withdrawal of a bed and Δt is the insertion or withdrawal time. Now $|\Delta B/B| = |\Delta I/I|$ so that

$$\dot{Q} = \frac{1}{\rho}\left(\frac{\Delta I}{I}\right)^2 \left(\frac{p}{2\pi}\right)^2 \frac{B^2}{(\Delta t)^2} \ . \tag{17}$$

If we integrate $\dot{Q}$ over the volume V of the winding, we obtain the total coupling power P :

$$P = f' \frac{2\mu_0}{\rho}\left(\frac{\Delta I}{I}\right)^2 \left(\frac{p}{2\pi}\right)^2 \frac{1}{(\Delta t)^2} \iiint_V \frac{B^2}{2\mu_0}\, d(\mathrm{vol}) \tag{18}$$

where f' is the volume fraction of conductor in the winding ($\pi/2\sqrt{3} = 0.907$).

The last term is a fraction g of the stored energy E of the magnet. Since coupling losses are present only when the bed is moving, the average coupling power per cycle is $2\,\Delta t/\tau$ times the power given in Eq. (18); here, τ is the cycle time. Thus, finally,

$$P = \frac{f'}{\pi^2}\frac{\mu_0 p^2}{\rho\tau\Delta t}\left(\frac{\Delta I}{I}\right)^2 gE \ . \tag{19}$$

The fraction g for our solenoid is 0.343. Accordingly, $gE = 20$ kJ.

The bulk of the coupling losses will come from the high-field region, where B is largest. A suitable value of ρ for copper in a 7-T field is about 5×10^{-10} ohm-m (RRR = 100). For p we use 10 strand diameters, i.e., 8 mm. The cycle time is 2 s, the insertion time 0.5 s. Then $P = 0.107$ W per bed or 0.214 W for both beds.

The total ac losses resulting from the motion of the beds should then be roughly 1 W, corresponding to a boiloff of liquid helium of 1.4 L/hr. Since the cross-sectional area of the helium pot above the magnet is 710 cm^2, this boiloff corresponds to a rate of drop of the helium level of 2 cm/hr. The height of the ullage volume above the magnet is

15 cm, so steady operation of no more than 7.5 hours is possible before the helium pot must be refilled.

8. RADIAL DESTABILIZING FORCE ON THE BED IN THE MAGNET

Owing to the increase in field as one moves radially outwards from the bore center, a bed is mechanically unstable when inserted in the magnet: if the bed suffers a small displacement from dead center, it will experience a magnetic force in the direction of the displacement that tends to increase the displacement further. This magnetic force, if inadequately restrained, will push the bed assembly against the wall of the bore tube, a circumstance that is highly undesirable. This unstable motion of the bed is restrained by the stiffness of the support tubes (one-inch, stainless-steel tubes). If the bearings that guide the support tubes can prevent rotation of the tubes (clamped boundary condition), the thickness of the tubes (25 mil) is sufficient for them to restrain the magnetic destabilizing force. If the bearings cannot prevent rotation of the tubes (pinned boundary condition), 25 mil in not sufficient for the tubes to restrain the magnetic destabilizing force.

The total force on the bed is given by Eq. (12a). Figure 11 shows a schematic depiction of the bed in the bore tube. The net transverse force on the bed is in the direction of the displacement OP of the bed center P from the bore center O. In the cross-sectional plane (b), we let the direction OP be the x-axis. The x-component of $n\,dS$ is then $R\cos\theta\,d\theta\,dz$, where R is the bed radius. Then the x-component of F is given by

$$F_x = MR \int_{-z_o}^{z_o} dz \int_0^{2\pi} d\theta \;\cos\theta\, B(r,z,\theta) \;. \tag{20}$$

By symmetry, ∇B vanishes at O; but O is neither a simple maximum nor a simple minimum, but rather a saddle point, being a minimum in the r-direction and a maximum in the z-direction. We therefore set

$$B = B_o - \frac{1}{2}\,c_1 z^2 + \frac{1}{2}\,c_2 r^2 \tag{21}$$

in the neighborhood of O. When Eq. (21) is inserted into Eq. (20), the first two terms make no contribution because for them the θ-integral vanishes. Therefore,

$$F_x = MRz_o c_2 \int_0^{2\pi} \cos\theta\; r^2 d\theta \;. \tag{22}$$

Applying the law of cosines to triangle OPQ, we see that

$$r^2 = R^2 + e^2 + 2Re\,\cos\theta \;. \tag{23}$$

Again the first two terms contribute nothing to the integral. We find finally that

$$F_x = MRz_0 \cdot 2eR\pi = MVc_2 e = MV\left(\frac{\partial^2 B}{\partial r^2}\right)_0 e \tag{24}$$

or in terms of the force per unit displacement

$$\frac{F_x}{e} = MV\left(\frac{\partial^2 B}{\partial r^2}\right)_0 \tag{25}$$

where V is the bed volume.

A calculation of the fields at points O, A, B, and C in Fig. 11a gives the results shown in Table 5.

Table 5. Results of field computation

Point	Field (T)	Fit (T)	Error in field deviation (%)
O	7.0000	7.0000	0
A	7.7478	7.8445	13
B	7.7478	7.3742	–20
C	6.6259	6.5297	26

A least-squares fit of Eq. (21) to the deviations of the field from B_0 at points A, B, and C gives $c_1 = 1501$ T/m and $c_2 = 654.4$ T/m. Using a bed volume of 228 cm^3 (3 in. in diameter by 5 cm long), we find from Eq. (25) that

$$\frac{F_x}{e} = 1.01 \times 10^5 \text{ N/M} = 576 \text{ lb/in.} \tag{26}$$

Figure 12 shows schematically the G-10 bed assembly, the magnet and the one-inch stainless-steel support tubes. At the attachment of the support tube to the bed assembly (point A), the tube will be considered as clamped, i.e., not able to rotate. At the bearing, we shall take the tube to act as though pinned. Then, the force per unit deflection of the bed with respect to the bearing is $3B/\ell^3$, where ℓ is the unsupported length of the tube and B is its flexural rigidity.

Now, $B = YI$, where Y is the elastic modulus of the tube material (200 GPa for stainless steel) and I is the moment of inertia of the tube cross section around an axis through its centroid and perpendicular to the plane of bending. For a thin tube of radius r and thickness t, $I = \pi r^3 t$. So for the tube to restrain the force given by Eq. (8), we must have

$$\frac{F_x}{e} = 3\pi\left(\frac{r}{\ell}\right)^3 Yt \ . \tag{27}$$

The unsupported length ℓ is about 14 in. so that $t = 1.18$ mm = 46.5 mil.

If the bearing clamps the tube against rotation, the force per unit deflection is four times larger than if the bearing merely pins the tube. Then the value of t required for mechanical stability is four times smaller, i.e., 11.6 mil.

9. LOCATION OF THE 5-GAUSS SURFACE

Since 5 Gauss is less than one ten-thousandth of the central field of the magnet, we can use the approximation that the magnet is a simple dipole located at the center point in determining the location of the 5-Gauss surface. The total dipole moment M of the magnet is given by

$$M = \frac{2\pi}{3} a^4 J\beta\left(\alpha^3 - 1\right) . \tag{28}$$

The magnetic field of such a dipole (assumed to be pointing in the z-direction) in cylindrical coordinates (r, z) is

$$B = \frac{\mu_0 J a^4}{3} \beta\left(\alpha^3 - 1\right) \frac{\left(r^4 + 4z^4 + 5z^2r^2\right)^{1/2}}{\left(r^2 + z^2\right)^{5/2}} . \tag{29}$$

On the axis ($r = 0$), the 5-Gauss point occurs 2.12 m from the magnet center. In the central plane ($z = 0$), the 5-Gauss point occurs 1.68 m from the center. In the diagonal plane ($r = z$), the 5-Gauss point occurs 1.96 m from the center. These three points come very close to lying on an ellipse. For practical purposes, then, the 5-Gauss surface is an ellipsoid of revolution whose major axis, 2.12 m long, is along the magnet axis and whose minor axes, 1.68 m long, are perpendicular to the magnet axis.

Since each iron piece is effectively two magnetic dipoles close together, the iron should not affect the field at great distances from the magnet center. As reference to the axial field profiles in Fig. 6 shows, the field on the magnet axis is not affected much by the presence of the iron beyond 35 or 40 cm from the center.

10. CONSTRUCTION OF THE MAGNET

Figure 13 shows the construction drawing submitted to prospective vendors. The construction contract was awarded to American Magnetics, Inc. of Oak Ridge, TN 37830. A number of small variations were introduced in the course of construction that are not shown in this figure. The most important of these are (1) the replacement of the screwed-down lid plate sealed with an indium gasket by a welded closure, and (2) the replacement of the six 1/4-in. support rods by a support tube. Figure 14 is a photograph of the completed magnet. Fig. 15 is a photograph of the closed helium pot that shows the following six tubes: (1) a 1.625-in. tube above the 27-pin electrical connector (the layout of which

is given in Table 5), (2) a 1-1/4-in. pressure relief pipe, and (3) four 1/2-in. pipes, two for the vapor-cooled leads, one for adding liquid helium, and one for venting vapor. These tubes all penetrate the lid of the 77-K tank. The pressure relief tube is surmounted by a BS&B 1-1/2-in., 10-psig burst disk assembly.

Owing to the thickness of the insulation provided by the manufacturer on the wire, the actual number of turns is 10,067 instead of the 13,263 calculated for the bare wire. This change in the number of turns requires that the operating current be raised from 85.2 A to 112 A. The inductance of the winding is reduced from 16.0 H to 9.22 H. (These latter figures refer to the bare coil without the iron end-pieces.)

The magnet acceptance test was carried out at American Magnetics, Inc. on August 11, 1993. The magnet suffered two training quenches on its first two current ramps, the first at 6.3 T, the second at 6.4 T. On the third current ramp, the magnet achieved the design field of 7.0 T. After the design field was reached, the third current ramp was continued, and the coil quenched at a central field of 7.6 T. A fourth current ramp was undertaken, and the coil reached a central field of 8.0 T without quenching. The fourth ramp was not continued beyond 8.0 T.

The current required to produce a central field of 7.1 T, namely, 107 A, compared favorably with that calculated, namely, 106 A. (The latter figure takes into account both the effect of the iron pole pieces and the effect of the smaller number of turns actually wound.)

Fig. 16 shows the measured field along the magnet axis. The circles and crosses show the field in two different series of measurements. The triangles show the field in a third series of measurements in which the Hall probe was moved off center in the direction opposite to the first two series. Comparison of the triangles with the other points shows that the zero position of the Hall probe was mislocated about 1 cm from the center of the magnet. The measurements were carried out at a current of 107 A (central field of 7.1 T). The calculations shown in Fig. 6 are for a current of 85.23 A for 13260 turns, corresponding to 112 A for 10067 turns. For comparison with the measurements, the theoretical curves should thus be lowered by about 5%. The measurements show clearly that although the iron does lower the out-of-bore field, the decrease is less than expected.

The calculated inductance of the coil without the iron pole pieces is 9.2 H. The inductance measured with the pole pieces is 12.4 H at zero field and 10.65 H at 7.0 T. The reduction from the zero-field value is due to the saturation of the iron at high field.

Cooldown from nitrogen temperature (77 K) to helium temperature (4.2 K) required 44 L of helium and took about 1-1/2 hours. It took another two hours to collect enough liquid to cover the magnet, but this was in a 16-in. dewar.

REFERENCES

1. P. Valaris, H. C. Kanithi, R. Macri, and B. A. Zeitlin, "A Statistical Evaluation of SSC Conductors Produced at IGC/ASI," IEEE Trans. Magn. MAG-27 (2): 1752–1754 (1991).
2. J. F. Kallsen, W, K. McDonald, and J. D. Geno, "SSC Type NbTi Superconductor Research Program at Teledyne SC," IEEE Trans. Magn. MAG-27 (2): 1799–1802 (1991).
3. L. Dresner, "Propagation of Normal Zones in Thermally Insulated Superconductors," Advances in Cryogenic Engineering 26: 647–653 (1980).
4. S. A. Elrod, J. R. Miller, and L. Dresner, "The Specific Heat of NbTi from 0 to 7 T between 4.2 and 20 K," Advances in Cryogenic Engineering 28: 601–610 (1982).
5. R. P. Reed and A. F. Clark, "Materials at Low Temperatures," American Society for Metals, Metals Park, OH, 44073, 1983.
6. A. Devred et al., "Development of Spontaneous Quenches in Full-Length SSC Dipoles," presented at the 1989 Particle Accelerator Conference, Chicago, March 20–23, 1989.
7. T. H. Fawzi and P. E. Burke, "The Accurate Computation of Self and Mutual Inductances of Circular Coils," IEEE Trans. Power Apparatus and Systems, PAS-97 (2): 464–468 (1978).

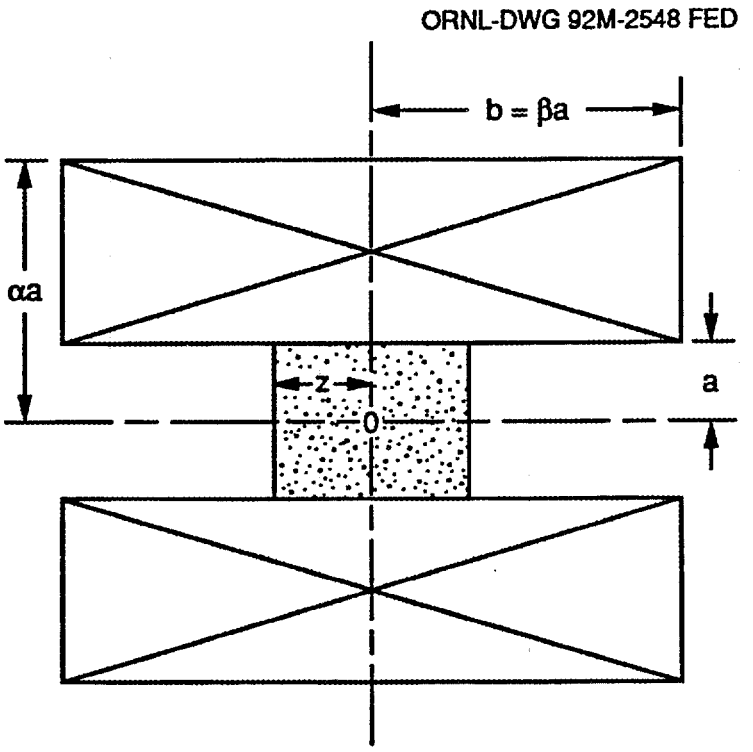

Fig. 1. A sketch of the magnet and bed defining the conventional shape factors α and β.

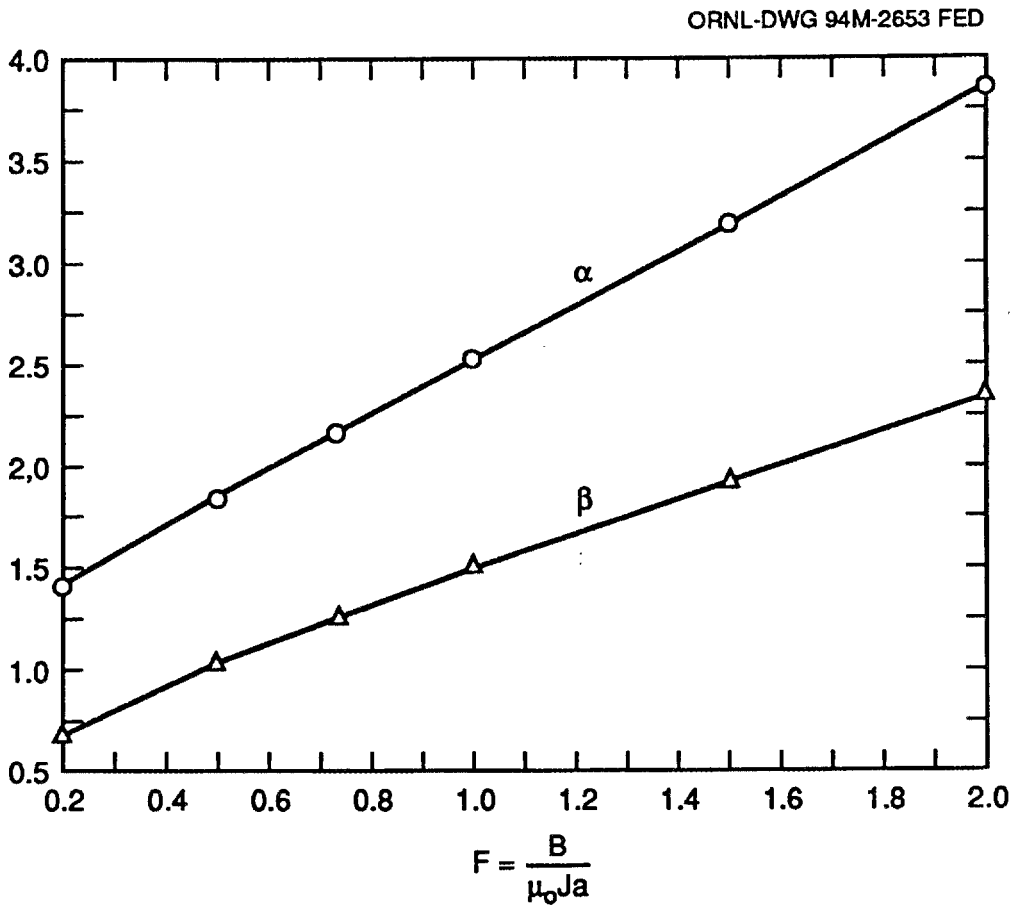

Fig. 2. The values of α and β that minimize $(\alpha^2 - 1)\beta$ plotted against $F(\alpha, \beta) = B_o/\mu_o Ja$.

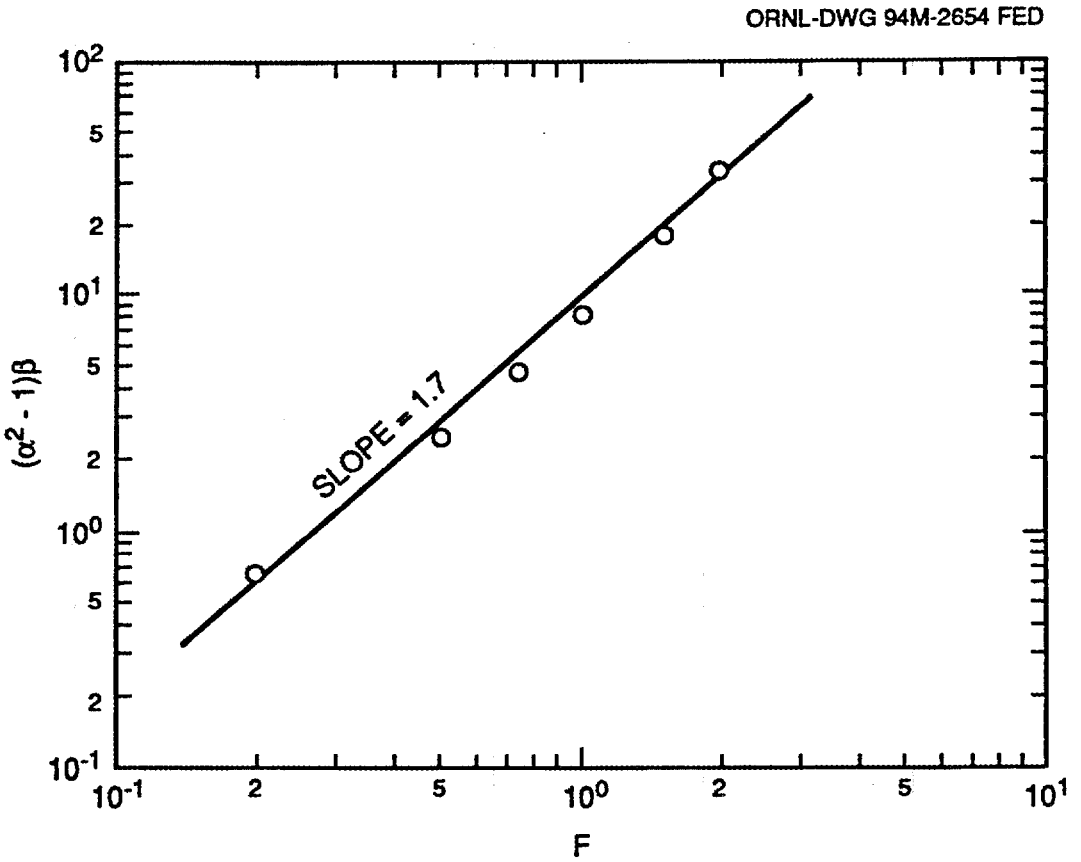

Fig. 3. The minimum value of $(\alpha^2 - 1)\beta$ plotted against $F(\alpha, \beta) = B_0/\mu_0 Ja$.

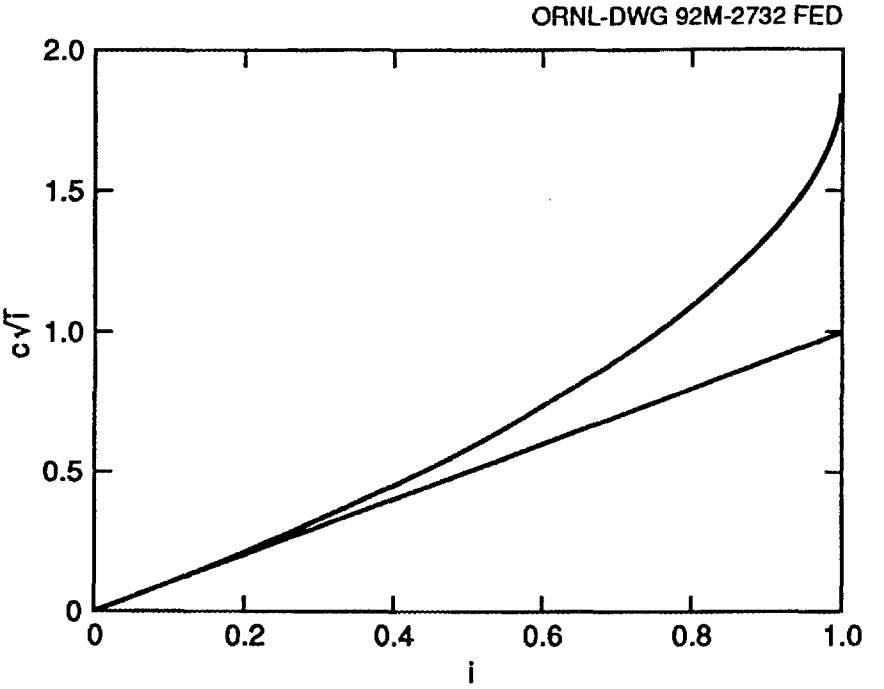

Fig. 4. The quantity $c\sqrt{i}$ plotted versus i [c is defined in Eq. (4b)]. Shown also is the straight line of slope 1 through the origin.

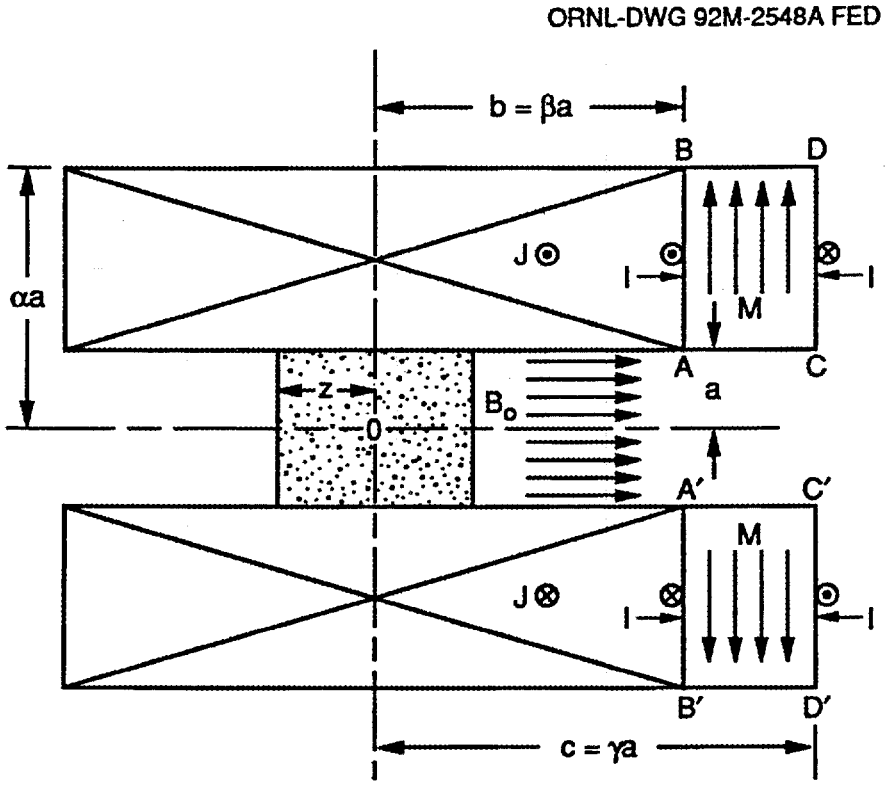

Fig. 5. A sketch of the magnet showing one of the soft iron end-flanges used as flux returns.

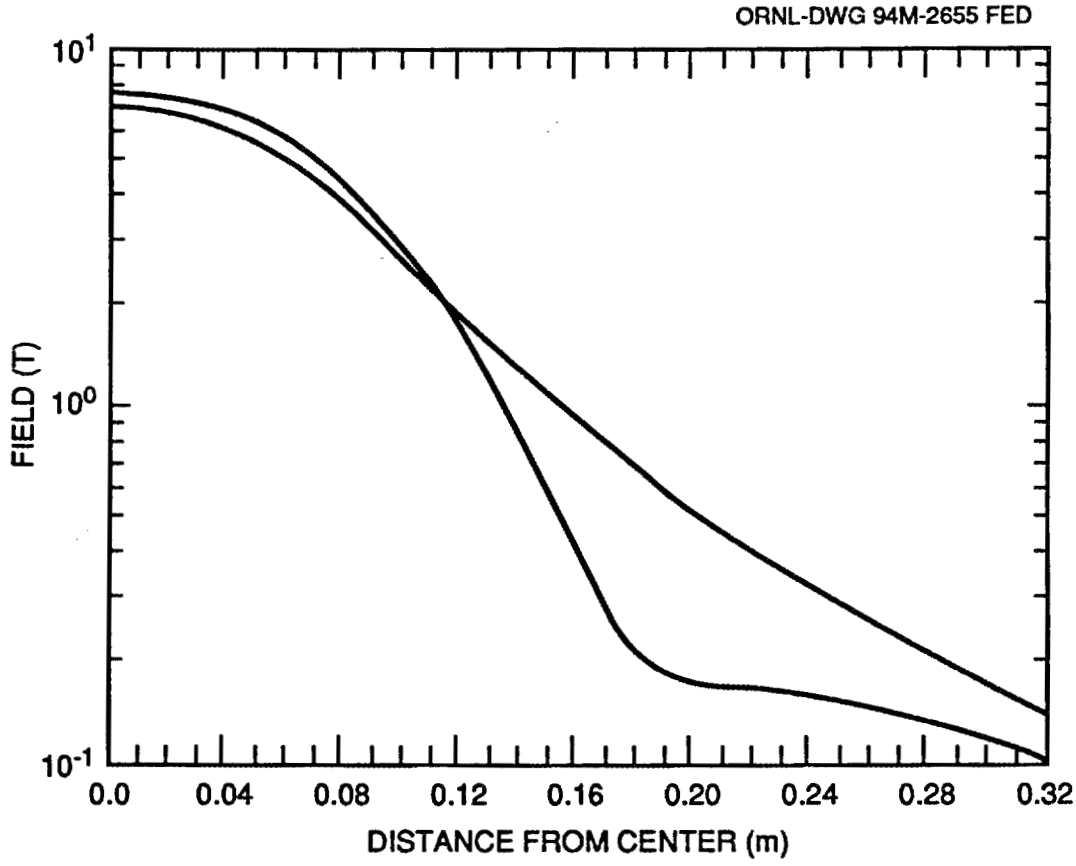

Fig. 6. The calculated on-axis field as a function of distance from the magnet center with and without the soft iron end-flanges.

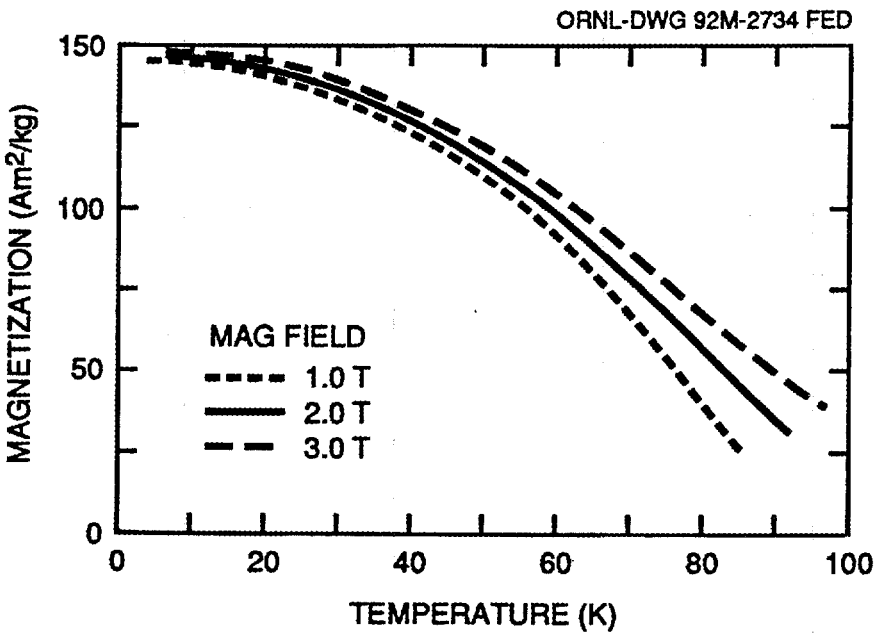

Fig. 7. The saturation magnetization of $GdNi_2$ as a function of temperature with field as a parameter.

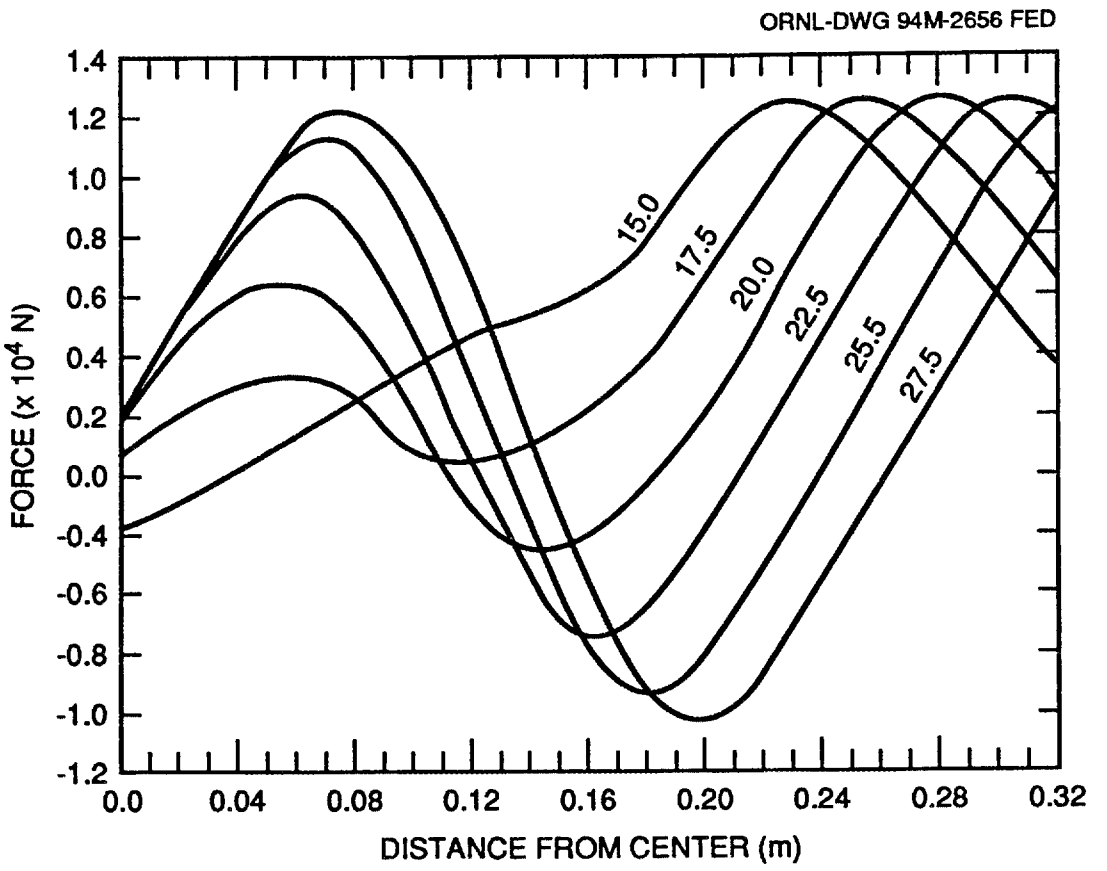

Fig. 8. The total force on a pair of rigidly connected beds as a function of the displacement of one of them from the center. The parameter labeling the curves is the bed separation in cm.

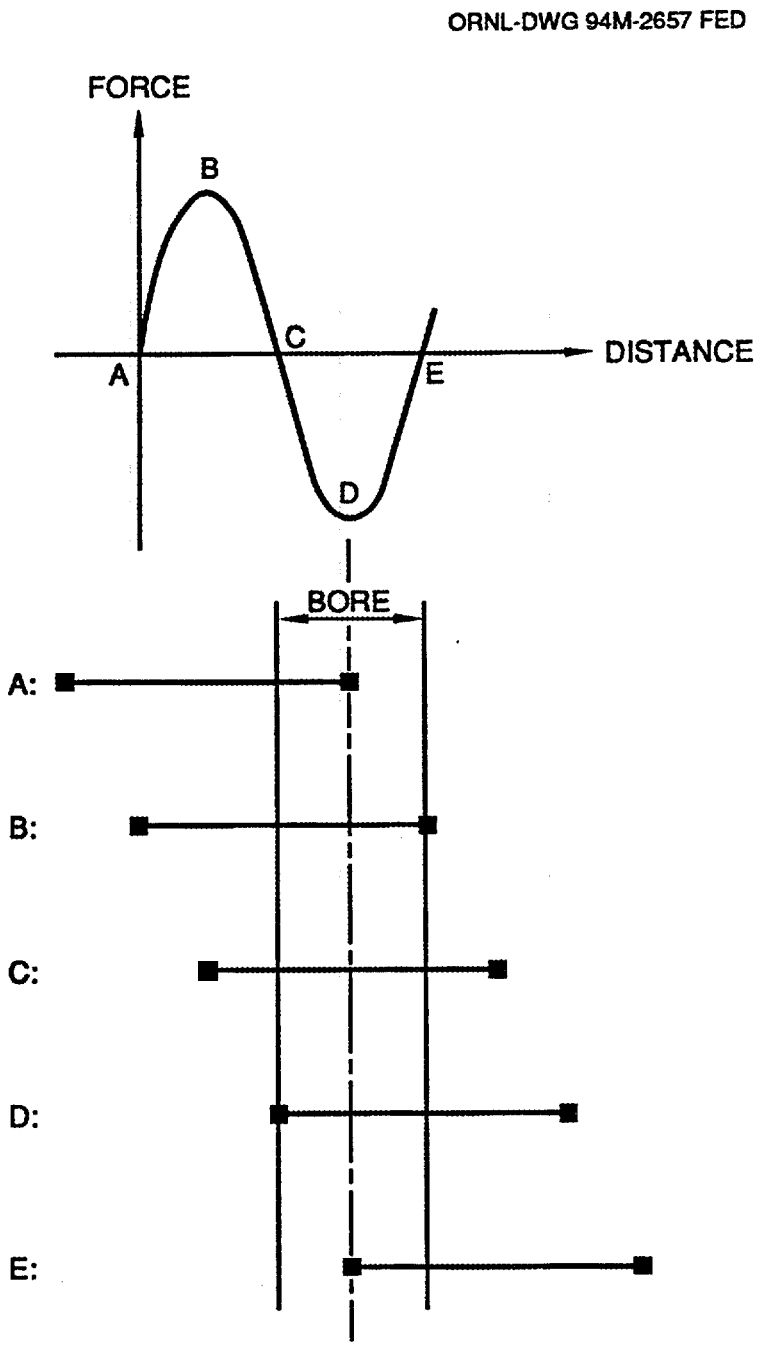

Fig. 9. An auxiliary sketch to aid in the interpretation of the curves in Fig. 8.

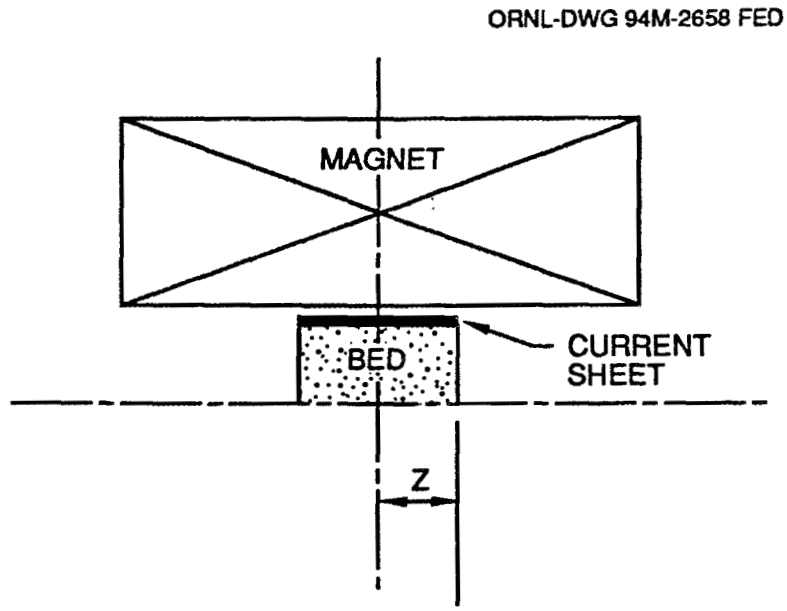

Fig. 10. A sketch showing the location of the current sheet that replaces the bed.

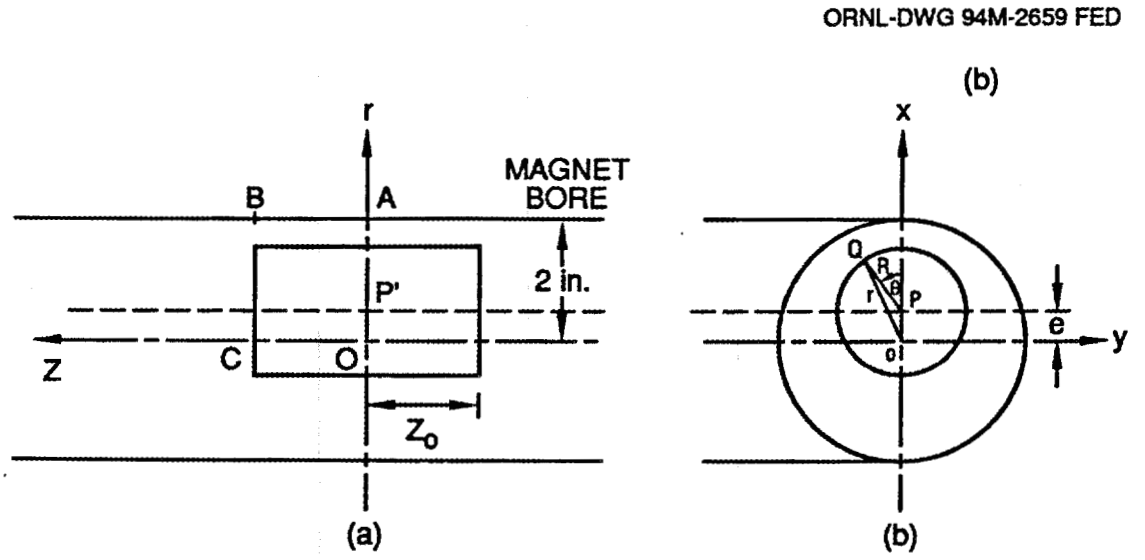

Fig. 11. A schematic depiction of the bed in the bore tube.

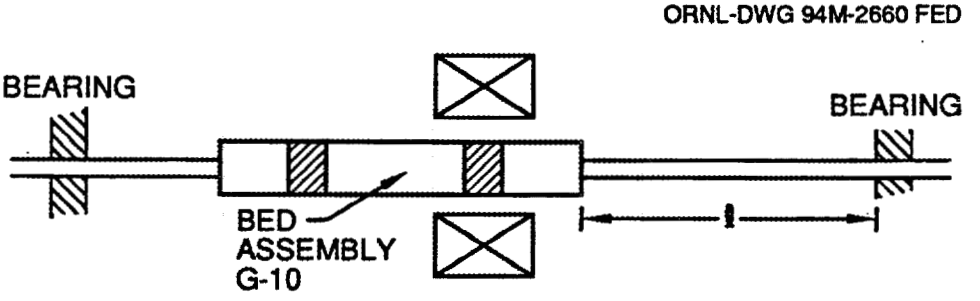

Fig. 12. A sketch of the bed assembly, support tubes, magnet, and bearings.

ORNL-DWG 94-2661 FED

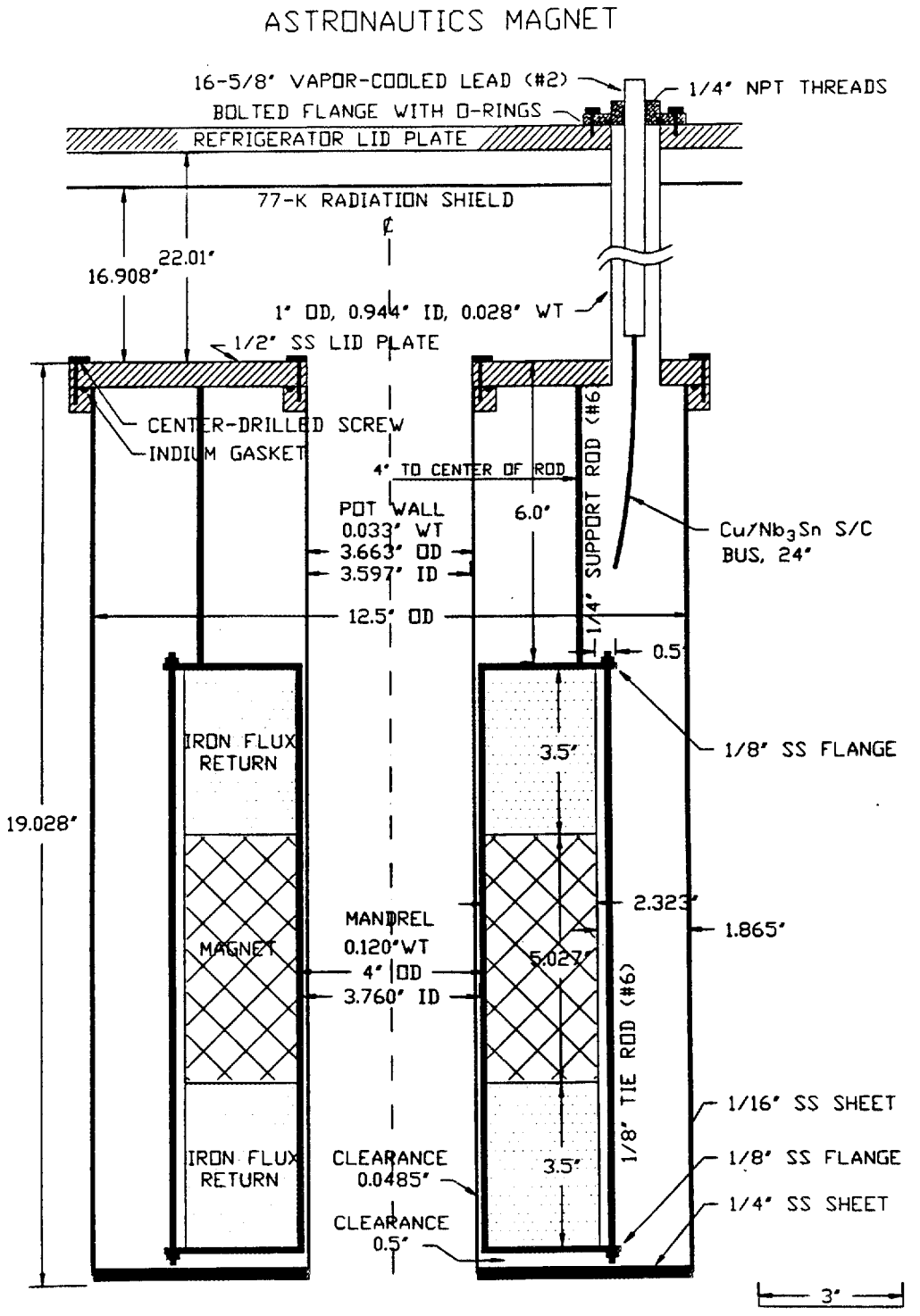

Fig. 13. The construction drawing of the magnet. A number of small variations were introduced in the course of construction that are not shown in this figure (see main text).

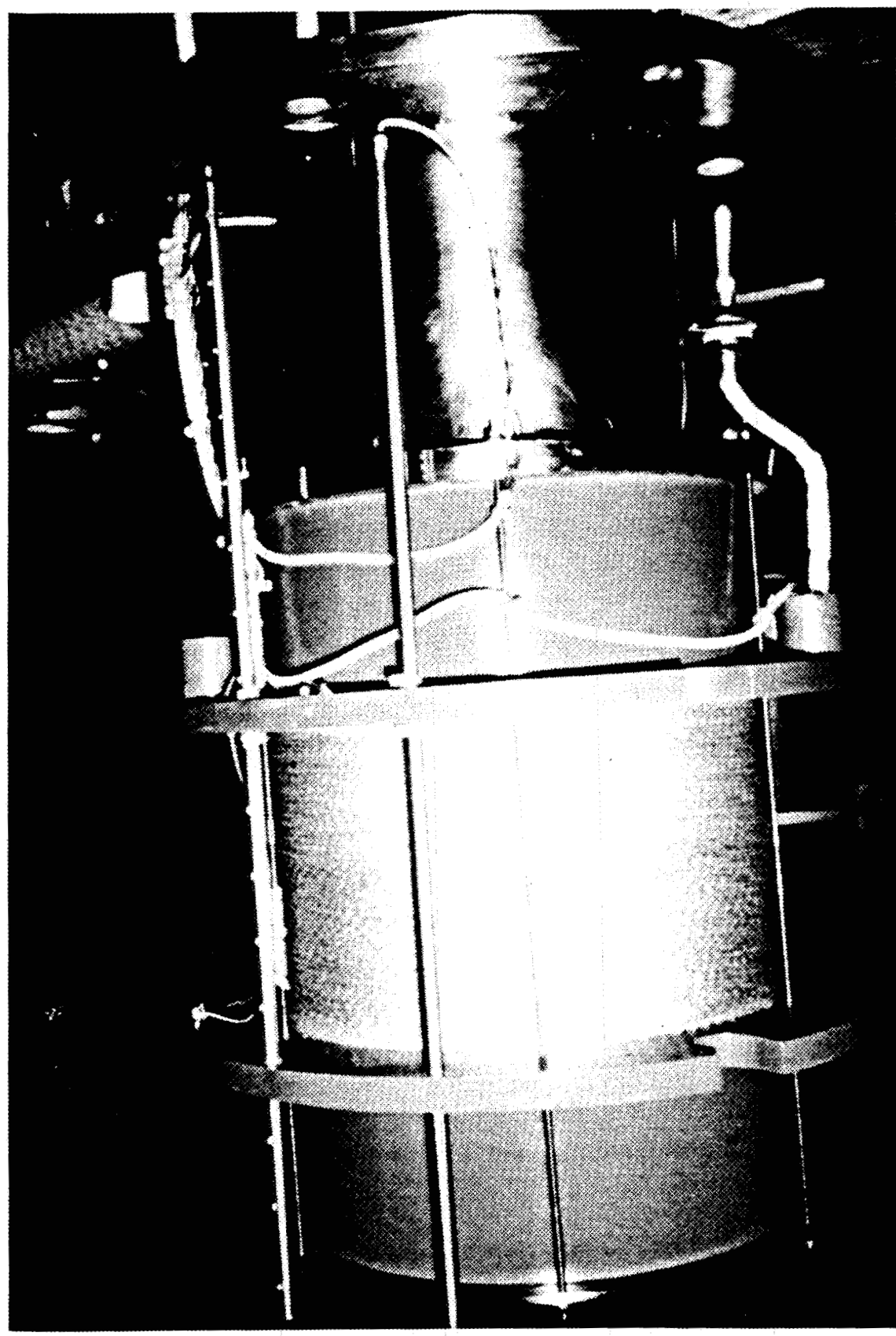

Fig. 14. A photograph of the completed magnet.

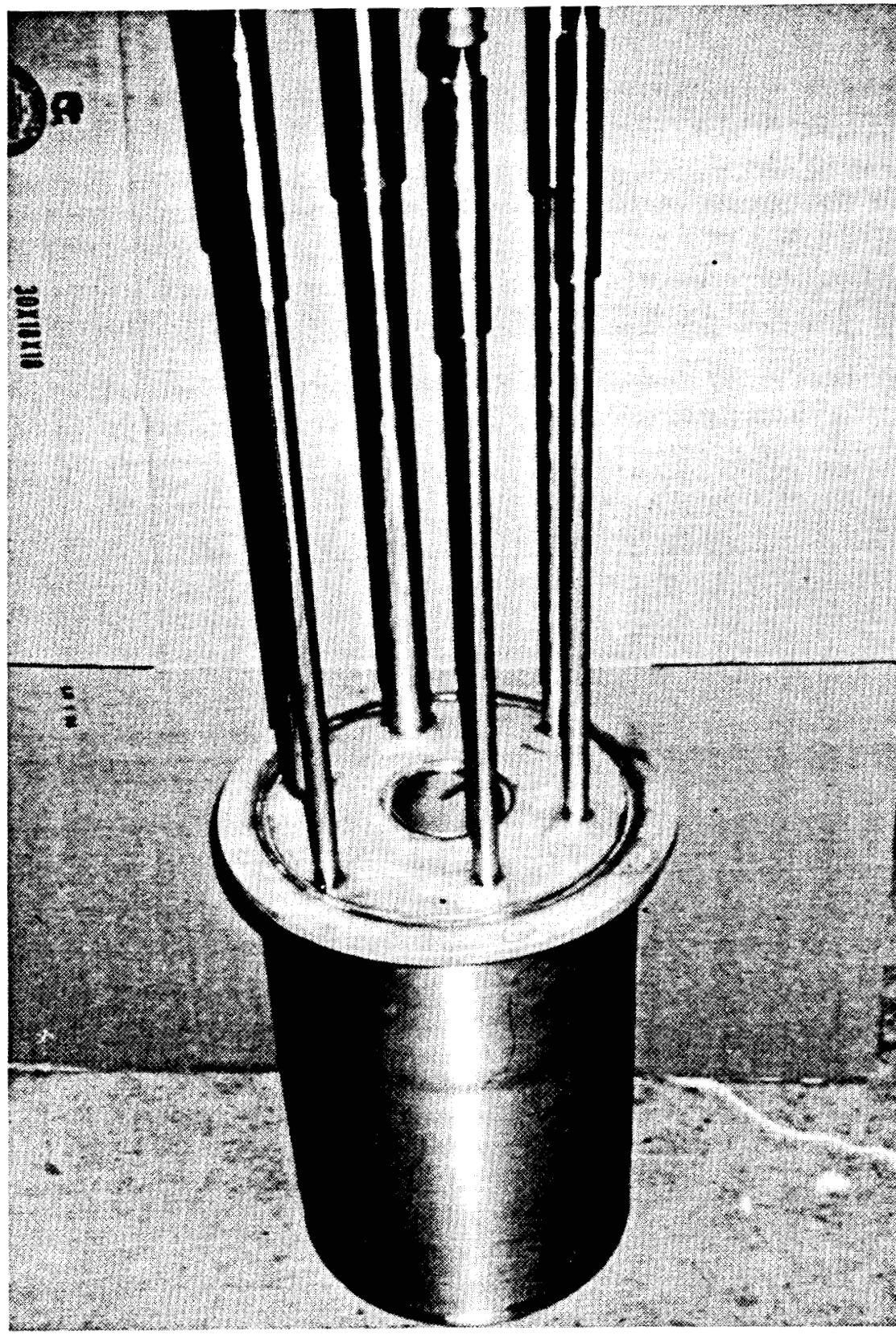

Fig. 15. A photograph of the closed helium pot showing the six tubes that connect the interior of the helium pot to the laboratory.

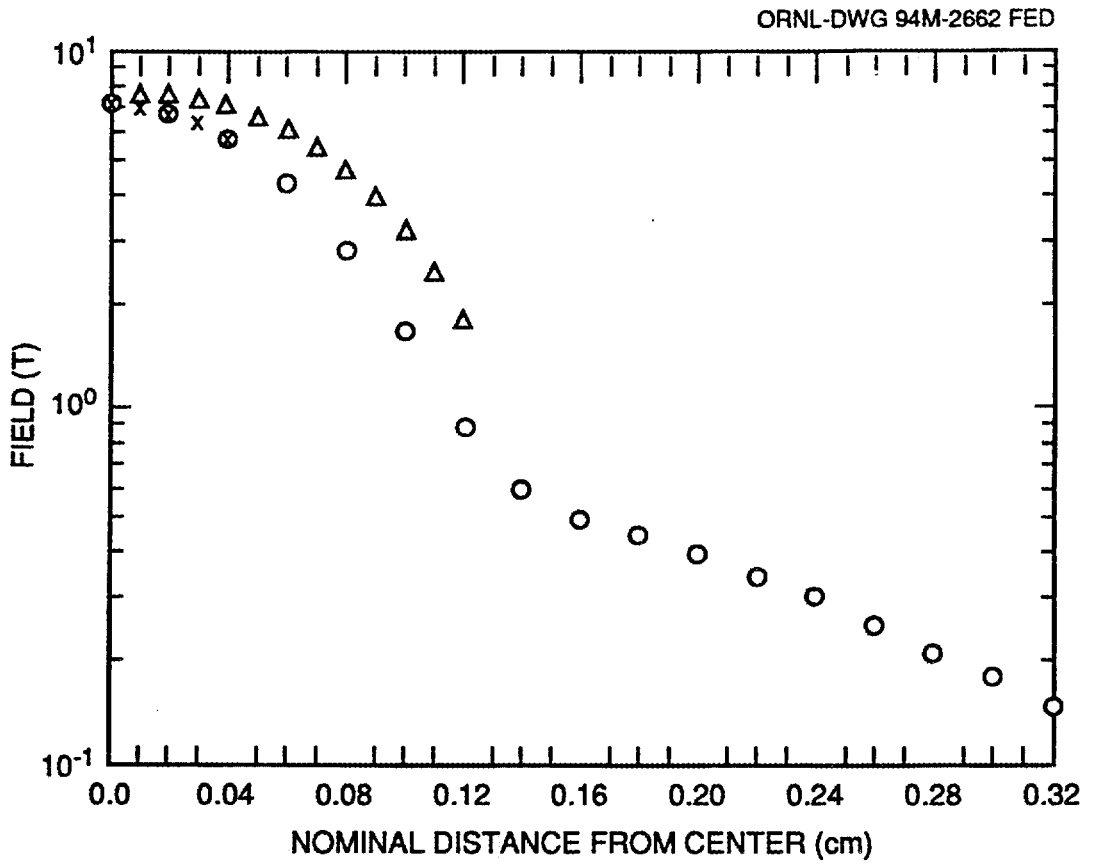

Fig. 16. The measured on-axis field as a function of distance from the magnet center with the soft iron end-flanges present.

INTERNAL DISTRIBUTION

1. J. Sheffield
2. M. S. Lubell
3–4. L. Dresner
5–6. R. A. Hawsey
7. R. W. Murphy
8. ORNL Patent Office
9. Laboratory Records, ORNL-RC
10. Engineering Technology/Fusion Energy Division Publications Office
11. Central Research Library
12. Document Reference Section
13–14. Laboratory Records Department
15. T. E. Shannon
16. W. L. Stirling
17. W. D. Nelson
18. A. C. Schaffhauser

EXTERNAL DISTRIBUTION

19. Office of Assistant Manager for Energy Research and Development, U.S. Department of Energy Field Office, Oak Ridge, P.O. Box 2000, Oak Ridge, TN 37831
20. Carl Zimm, Astronautics Technology Center, 5800 Cottage Grove Road, Madison, WI 53716
21. Richard Foster, Astronautics Technology Center, 5800 Cottage Grove Road, Madison, WI 53716
22. L. M. Lawton, Jr., Astronautics Technology Center, 5800 Cottage Grove Road, Madison, WI 53716
23. Dr. James G. Daley, Office of Energy Management, DOE, EE-142, 6H-034/FORS, 1000 Independence Avenue, SW, Washington, DC 20585

24–25. Office of Scientific and Technical Information, P.O. Box 62, Oak Ridge, TN 37831